Monolithically integrated dual-wavelength photodetector based on a step-shaped Fabry-Pérot filter

Xinye Fan (范鑫烨)*, Yongqing Huang (黄永清), Xiaomin Ren (任晓敏), Xiaofeng Duan (段晓峰), Fuquan Hu (胡服全), and Qi Wang (王 琦)

State Key Laboratory of Information Photonics and Optical Communications, Beijing University of Posts and Telecommunications, Beijing 100876, China

**Corresponding author: fanxinye@yeah.net*

Received April 5, 2012; accepted May 17, 2012; posted online September 28, 2012

A novel long wavelength photodetector with dual-wavelength spectral response is designed and fabricated using a step-shaped Fabry-Pérot (F-P) filter structure. The step-shaped GaAs/AlGaAs distributed Bragg reflectors and the InP PIN photodetector are grown on a GaAs substrate using low pressure metal organic chemical vapor deposition. High quality GaAs/InP heteroepitaxy is realized by employing a thin low temperature buffer layer. The photodetector structure is optimized by theoretical simulation. This device has a dual-peak distance of 19 nm (1 558 and 1 577 nm). The 3-dB bandwidth of 16 GHz is simultaneously obtained with peak quantum efficiencies of 8.5% and 8.6% around 1 558 and 1 577 nm, respectively.

OCIS codes: 040.5160, 050.2230, 120.2440.
doi: 10.3788/COL201210.110402.

Dual-wavelength photodetectors in the 1.3- or 1.55-μm wavelength regions have significant potential in optical-fiber communication systems, especially for numerous microplate-based applications that aim to reduce optical interference caused by crosstalk, dispertion, or other impact factors of energy transmission and loss in optical transmission systems[1−5]. The operation of dual-wavelength response has been demonstrated in several structures, including a taper substrate[6], two stacks of quantum-well structures[7], and two photodiodes[8]. However, the attractive approach of realizing a dual-wavelength photodetector with step-shaped Fabry-Pérot (F-P) filter has yet to be reported.

Furthermore, the distributed Bragg reflectors (DBR) in these F-P filters have been made from various materials, such as AlInGaAs/InAlAs[9], InGaAsP/InP[10], metamorphic GaAs/AlAs[11], and dielectric mirrors[12]; however, they all have the common problem of poor refractive index contrast. Among these candidates, GaAs/AlGaAs are the most promising DBRs because of their good electronic properties, reasonably low carrier recombination rates, and good refractive index contrast. However, for long wavelength (from 1.3 to 1.8 μm) photodetector fabrication, the PIN structure is preferred to be InP based. Several approaches on integrating GaAs/AlGaAs DBRs with the InP-based PIN photodetectors have been investigated, such as employing a thin, low temperature buffer layer[13], fusing the InP-based active region with GaAs-based DBRs[14], and growing metamorphic GaAs/AlGaAs DBRs on InP-based materials[15]; these have been realized in tunable photodetectors[13], resonant-cavity-enhanced photodetectors[16], and vertical-cavity surface-emitting lasers[17], respectively.

In this letter, we propose a novel dual-wavelength photodetector realized by integrating a step-shaped GaAs based F-P filter with an InP-based PIN photodetector. High quality GaAs/InP heteroepitaxy is realized using a thin, low temperature buffer layer. We design and fabricate monolithically integrated step-shaped photodetectors that exhibit high spectrum and speed responses.

Figure 1 shows the proposed bottom-injection type photodetector with step-shaped F-P filter. The incident light passes through the step-shaped filter into the PIN photodetector. The GaAs-based filter was constructed using a five-wave-thick GaAs cavity layer and two distributed Bragg reflectors. The bottom and top reflectors consisted of 22 pairs of quarter-wave stacks of GaAs and AlGaAs layers, respectively. Then an InP-$In_{0.53}Ga_{0.47}As$-InP PIN structure was then integrated with the step-shaped F-P filter.

We used the transfer matrix method to simulate the spectral response. The absorption coefficient of active layer was 0.68 μm^{-1}. If the GaAs cavity had two

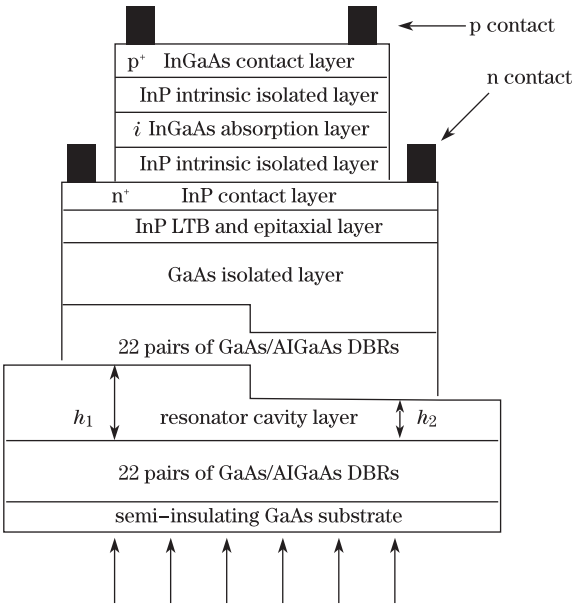

Fig. 1. Schematic structure of the photodetector with step-shaped filter.

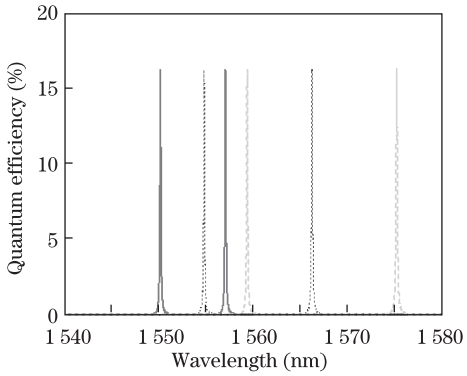

Fig. 2. Quantum efficiency of the dual-wavelength photodetectors with step-shaped F-P filter (Δh has three different lengths, a=10 nm (solid curve), b=20 nm (dotted curve), and c=30 nm (dash curve)).

different lengths h_1, h_2 (Fig. 1), the total output response was superimposed by the two responses, each taking 50% weight to the final superimposition. The dual-wavelength response is dependent on the proper change in thickness, which is $\Delta h = h_1 - h_2$, and proper Δh can lead to a proper dual-peak distance. Although the dual-wavelength response can still be attained, the dual-peak distance of the spectral response becomes very narrow at about 9 nm between 1 551 and 1 560 nm when Δh is 10 nm. Then, we obtain the quantum efficiency with the change of the dual-peak distance (Fig. 2). Next, we enlarged the dual-peak distance by designing the step distance of the GaAs cavity layer with the different lengths of a, b, and c at 0, 20, and 30 nm, respectively. From these, dual-peak distances of 7, 14, and 16 nm, respectively, are obtained. The dual-peak distance widens when the Δh increases.

The structure was grown through low pressure metal organic chemical vapor deposition (LP-MOCVD) on a semi-insulating GaAs substrate. Our MOCVD used Trimethylindium (TMIn) and Trimethylgallium (TMGa) as group-III precursors; AsH_3 and PH_3 as group-V precursors; as well as SiH_4 and diethylzinc (DEZn) as n-type and p-type dopant precursors. The growth procedure was divided into three parts. First, 22 pairs of quarter-wave stacks of GaAs/AlGaAs layers (λ_0=1 550 nm) and an 800-nm GaAs cavity layer were grown on a semi-insulating GaAs substrate. Second, four steps were etched on the epitaxial layer surface of the GaAs cavity using a $H_2SO_4/H_2O_2/H_2O$ solution. The step height and width were 20 and 800 nm, respectively. Third, after degreasing in organic solvents, another 800-nm GaAs cavity layer and 22 pairs of quarter-wave stacks of GaAs/AlGaAs layers were regrown. Next, a 48-nm InP low temperature buffer (LTB) layer was grown at 723.15 K. This thin LTB layer realized the high quality GaAs/InP heteroepitaxy growth. The PIN structure of the photodetectors was grown subsequently, which consisted of several layers: 256-nm n-type InP, 468-nm InP spacer, 400-nm $In_{0.53}Ga_{0.47}$ As absorber, 240-nm InP spacer, and 200-nm p-type InGaAs. Finally, a 120-nm InP cap layer was grown.

The device was fabricated through the following procedures. The 120-nm InP cap layer was selectively removed in the HCl/H_3PO_4 solution. After lithography, Ti and Au were evaporated and patterned by a lift-off process to form an annular p+ Ohmic contact with an internal diameter of 30 μm. A 42-μm diameter top round mesa was formed by etching down to the n-type InP contact layer. The InP and InGaAs layers were selectively removed from the HCl/H_3PO_4 and $H_2SO_4/H_2O_2/H_2O$ solutions, respectively. The etch rate was highly controlled by inspecting the test samples. The n+ Ohmic contact was achieved by a Pt/Ti/Pt/Au lift-off. Then a photodefinable polyimide layer was used for passivation/planarization prior to the deposition of the metal coplanar electrode; this was then annealed for passivation. Ti/Au was evaporated and patterned by a lift-off process to form the electrodes. Finally, a novel metal ground-signal-ground (GSG) electrode was linked to the photodetector for high-speed interconnection. After polishing, the device was considered complete. Figure 3 shows the optical microscope images of the device (Φ 15 and Φ 40 μm).

Figure 4 shows the double-crystal X-ray diffraction scans of the epitaxial layer, in which the left peak is introduced by the InP-based PIN structure; the full-width at half-maximum (FWHM) value is 480″. The high quality InP/GaAs heteroepitaxy growth is realized. Based on the GaAs substrate, the two peaks on the right correspond to the GaAs/AlGaAs F-P cavities, respectively, and the left peak corresponds to AlGaAs, because its crystal lattice constant is larger than GaAs.

The spectral response was measured in the 1 460–1 610-nm wavelength range using an Anritsu Tunics SCL tunable laser with a single-mode fiber pigtail as the light source.

The photodetector was back-illuminated vertically. An input beam was obtained by collimating the light from the fiber with a fiber collimator. Figure 5 shows the

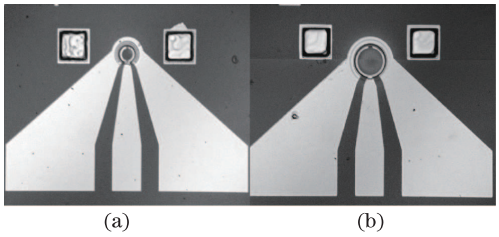

Fig. 3. Optical micrograph of the fabricated step-shaped photodetector showing (a) Φ 5-μm photosensitive area and (b) Φ 40-μm photosensitive area.

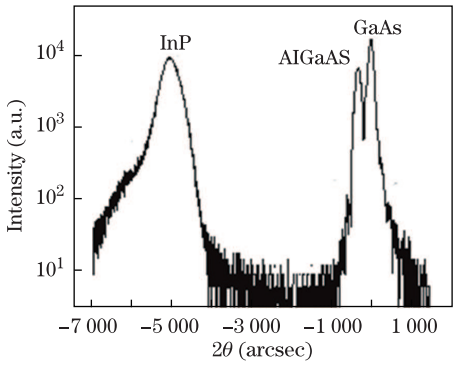

Fig. 4. Double crystal X-ray diffraction ω-2θ scans.

spectral response of the device, indicating the peak wavelengths of 1 558 and 1 577 nm. The right curve corresponds to the as-grown wafer, and the other corresponds to the cumulative recess etch of 20 nm in the F-P cavity. The spectral linewidth is less than 0.5 nm (FWHM), which is mainly dependent on the number of DBR layers. Thus, more pairs of DBR layers are required for a narrower linewidth. This device has a dual-peak distance of 19 nm (1 558 and 1 577 nm). The peak quantum efficiencies are 8.5% and 8.6% around 1 558 and 1 577 nm, respectively.

The bandwidths associated with the carrier transit-time and the RC time-constant determine the high speed performance of a photodetector. The bandwidths were measured with a tunable laser and an Agilent E8363C network analyzer. The device was contacted by a microwave probe with a 50-Ω characteristic impedance and was biased through an internal bias tee. Figure 6 shows the measured frequency response, the 3-dB bandwidth for the Φ 15 and Φ 40 μm photosensitive areas achieve 16 and 13 GHz, respectively, at a 200-nm i-region thickness and 5.52×10^6-cm/s average saturation drift velocity. Thus, a smaller area is preferred in increasing the response speed of the photodetector.

The room temperature current-voltage characteristic of the device was measured without illumination. The dark current slowly increases from 2 nA (at 0 V) to 20 nA (at 6 V) (Fig. 7). At larger reverse biases, the dark current increases more rapidly due to tunneling at a higher electric field. The dark current is 10 nA at a reverse bias of 3 V (Fig. 7 inset). Several sources contributed to the dark current, including the imperfect surface passivation[18], diffusion current, generation recombination current, and tunneling current at high bias voltages[19]. The generation recombination current is mainly caused by the background dopant and the mismatch dislocations[20]. Using a thin LTB layer, the high quality heteroepitaxy growth reduced the generation recombination current due to lower mismatch dislocations.

In conclusion, we propose a novel photodetector with dual-wavelength spectral response by designing the photodetector structure and adjusting the thickness of the step distance of the GaAs cavity. The dual-peak distance widens as the Δh increases upon device optimization using the transfer matrix method. We also demonstrate a high speed, high efficiency, and dual wavelength photodetector using the step-shaped structure. Furthermore,

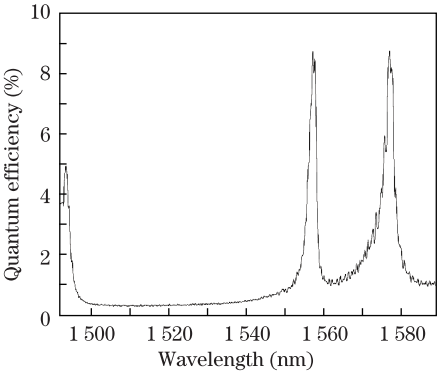

Fig. 5. Measured response spectrum of the fabricated dual-wavelength photodetector.

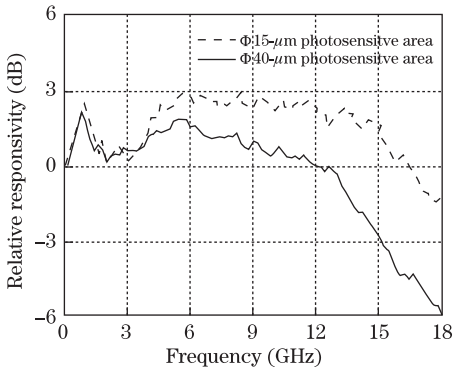

Fig. 6. Measured frequency response of the photodetectors showing Φ 15-μm photosensitive area and Φ 40-μm photosensitive area.

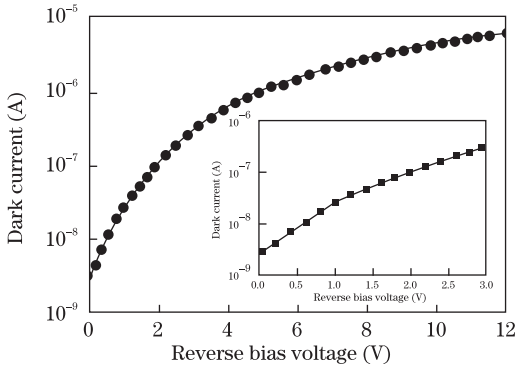

Fig. 7. Measured dark current against the reverse bias of the device. Inset: dark current for reverse bias from 0 to 3 V.

we obtain a dual-peak distance of 19 nm, peak quantum efficiency of over 8%, and 3-dB bandwidth over 16 GHz.

The authors wish to thank Yongqing Huang, Xiaofeng Duan, and Xiaomin Ren for their helpful discussions. This work was supported by the National "973" Program of China (No. 2010CB327600), the National Natural Science Foundation of China (No. 61020106007), the Fundamental Research Funds for the Central University (No. BUPT2011RC0403), the National "863" Program of China (No. 2007AA03Z418), the 111 Project of China (No. B07005), and the Program for Changjiang Scholars and Innovative Research Team in University MOE, China (No. IRT0609).

References

1. M. Zhang, D. N. Wang, H. Li, W. Jin, and M. S. Demokan, IEEE Photon. Technol. Lett. **14,** 92 (2002).
2. S. D. Roh, T. S. Yeoh, and R. B. Swint, IEEE Photon. Technol. Lett. **12,** 1307 (2000).
3. F. Coppinger, J. Yeh, J. Singh, G. Dagnall, L. Chen, and D. Piehler, in *Proceedings of Optical Fiber Communication Conference* 734 (2003).
4. J. J. Yu and X. Zhou, IEEE Commun. Mag. **48,** S56 (2010).
5. T. H. Wood, A. K. Srivastava, J. L. Zyskind, J. W. Sulhoff, and C. Wolf, in *Proceedings of Optical Fiber Communication* 320 (1997).
6. J. H. Lv, H. Huang, Y. Q. Huang, X. M. Ren, Q. Wang and S. W. Cai, IEEE Trans. Electron. Dev.

55, 322 (2008).

7. M. Z. Tidrow, J. C. Chiang, S. S. Li, and K. Bacher, Appl. Phys. Lett. **70,** 859 (1997).
8. J. C. Campbell, C. A. Burrus, and J. A. Copeland, IEEE Trans. Electron. Dev. **30,** 1610 (1983).
9. R. J. Stone, R. F. Nabiev, J. Boucart, W. Yuen, P. Kner, G. S. Li, R. Carico, L. Scheffel, M. Jansen, D. P. Worland, and C. J. Chang-Hasnain, IEEE Electron. Lett. **36,** 1793 (2000).
10. S. Z. Zhang, N. M. Margalit, T. E. Reynolds, and J. E. Bowers, IEEE Photon. Technol. Lett. **9,** 374 (1997).
11. W. Yuen, G. S. Li, R. F. Nabiev, J. Boucart, P. Kner, R. J. Stone, D. Zhang, M. Beaudoin, T. Zheng, C. He, and C. J. Chang-Hasnain, Electron. Lett. **36,** 1121 (2000).
12. W. Ren, P. Tao, Z. Tan, Y. Liu, and S. Jian, Chin. Opt. Lett. **7,** 775 (2009).
13. X. F. Duan, Y. Q. Huang, X. M. Ren, H. Huang, S. X. Xie, Q. Wang, and S. W. Cai, Opt. Express **18,** 5879 (2010).
14. X. F. Duan, Y. Q. Huang, X. M. Ren, H. Huang, S. X. Xie, Q. Wang, and S. W. Cai, J. Lightwave Technol. **27,** 4697 (2009).
15. W. Yuen, G. S. Li, R. F. Nabiev, J. Boucart, P. Kner, R. J. Stone, D. Zhang, M. Beaudoin, T. Zheng, C. He, and C. J. Chang-Hasnain, Electron. Lett. **36,** 1121 (2000).
16. X. F. Duan, Y. Q. Huang, and X. M. Ren, Q. Wang, and S. W. Cai, IEEE Trans. Electron. Dev. **58,** 3948 (2011).
17. Y. Ohiso, H. Okamoto, and R. Iga, IEEE J. Quantum Electron. **37,** 1194 (2001).
18. K. Kato, IEEE Trans. Microw. Theory Technol. **47,** 1265 (1999).
19. W. A. Wohlmuth, J. W. Seo, P. Fay, C. Caneau, and I. Adesida, IEEE Photon. Technol. Lett. **9,** 1388 (1997).
20. J. H. Jang, G. Cueva, D. C. Dumka, W. E. Hoke, and P. J. Lemonias, IEEE Photon. Technol. Lett. **13,** 151 (2001).